Original Paper

Marko Komac · Rachel Holley · Pooja Mahapatra · Hans van der Marel · Miloš Bavec

Coupling of GPS/GNSS and radar interferometric data for a 3D surface displacement monitoring of landslides

Abstract Persistent scatterer interferometry (PSI) is capable of millimetric measurements of ground deformation phenomena occurring at radar signal reflectors (persistent scatterers, PS) that are phase coherent over a period of time. However, there are also limitations to PSI; significant phase decorrelation can occur between subsequent interferometric radar (InSAR) acquisitions in vegetated and low-density PS areas. Here, artificial amplitude- and phase-stable radar scatterers may have to be introduced. I2GPS was a Galileo project (02/2010–09/2011) that aimed to develop a novel device consisting of a compact active transponder (CAT) with an integrated global positioning system (GPS) antenna to ensure millimetric co-registration and a coherent cross-reference. The advantages are: (1) all advantages of CATs such as small size, light weight, unobtrusiveness and usability with multiple satellites and tracks; (2) absolute calibration for PSI data; (3) high sampling rate of GPS enables detection of abrupt ground motion in 3D; and (4) vertical components of the local velocity field can be derived from single-track InSAR line-of-sight displacements. A field trial was set to test the approach at a potential landslide site in Potoška planina, Slovenia to evaluate the applicability for operational monitoring of natural hazards. Preliminary results from the trial highlight some of the key considerations for operational deployments in the field. Ground motion measurements also allowed an assessment of landslide hazard at the site and demonstrated the synergies between InSAR and GPS measurements for landslide applications. InSAR and GPS measurements were compared to assess the consistency between the methods from the slope mass movement detection aspect.

Keywords Persistent scatterers · Compact active transponders · GPS · Landslide · Monitoring · Slovenia

Introduction

In the past 15 years radar interferometry (InSAR) has been used for variety of surface change detection purposes, from hydrology (Declerq et al. 2005; Ludwig and Schenider 2006), mining subsidence (Carnec and Delacourt 2000), glaciology (Mohr and Madsen 2000), ecology (Borgeaud and Wegmüller 1997), volcanology (Salvi et al. 2004), monitoring of slow landslides (Squarzoni et al. 2003; Hilley et al. 2004; Bovenga et al. 2006; Farina et al. 2006; Hole et al. 2011; Žibret et al. 2012), to tectonics (Komac and Bavec 2007; Žibret et al. 2012). InSAR technique was further developed to detect differences between interferometric pairs (differential InSAR, DifSAR) and to detect long-term differences in interferometric images (persistent scatterer interferomety).

The NAVSTAR Global Positioning System (GPS) was designed as an all-weather space-based navigation system by the US Department of Defense for both military and civilian navigation needs. Already early on, it was realised that carrier-phase observations can be used to determine relatively short baselines between two receivers with millimetre accuracy (Bossler et al. 1980; Remondi 1985). The establishment of the International GNSS Service (IGS) in 1994 made it possible to obtain millimetre accuracies on a global scale (Mueller and Beutler 1992; Dow et al. 2009), leading to significant improvements in the International Terrestrial Reference Frame (ITRF) and numerous high-precision geodetic and geodynamics applications (Teunissen and Kleusberg 1998).

The driving idea of I2GPS project was to combine the two technologies—GPS/global navigation satellite system (GNSS) and InSAR—co-register the measurements and use them for monitoring slowly moving landslides in 3D. For the purpose of the project, two trials at different test sites were performed, a 'laboratory trial' in Delft (NL) to validate the capabilities of the technology (Mahapatra et al. 2011) and a potential landslide site in Potoška planina (Slovenia) to evaluate the applicability for operational monitoring of natural hazards. The results of the first, 'laboratory trial' are not elaborated in this paper. As the second trial is still ongoing, we present here the interim, yet still interesting, results acquired within the project that enabled the development of a tool that allowed the co-registered GPS/GNSS and InSAR measurements—a I2GPS unit—and assessment of its applicability for landslide monitoring.

Local setting

Geology and geography

The key aim of the Slovenian field trial was to demonstrate that the system developed (a unit for collecting co-registered GNSS and InSAR data) is able to respond to specific user needs; in this case, to provide useful measurements of landslide and tectonic motion in an operational setting.

The chosen landslide site lies above the village of Koroška Bela, on the outskirts of the town of Jesenice in the Karavanke Mountain area of north-western Slovenia (Fig. 1). The Potoška Planina landslide is known to have produced at least four historical debris flows (Jež et al. 2008), some of which caused significant damage to a village down-slope that today has 2,000 inhabitants. A slide in the eighteenth century caused partial or total destruction of 40 buildings, and landslides of the same or greater mass could endanger the village in the future. Current activity on the slide is presumed to be active slow-motion slip. In the Alpine area, landslides and debris flows present serious danger to infrastructure and inhabitants (Mikoš et al. 2012). Implementing tools and field trials presented here could be used as complementary tool to reduce hazards due to slope mass movements.

The main part of the site occupies a gently sloping area at the foot of a steep limestone ridge. The lower, south-eastern section of the site is dissected by a steep-sided ravine, which broadens and levels out to form the main area of the landslip. Any debris slipping from the landslip would be funnelled down this ravine towards the village (Fig. 2), if conditions allow in a form of a debris flow. The average altitude of the site is 1250 m above sea level.
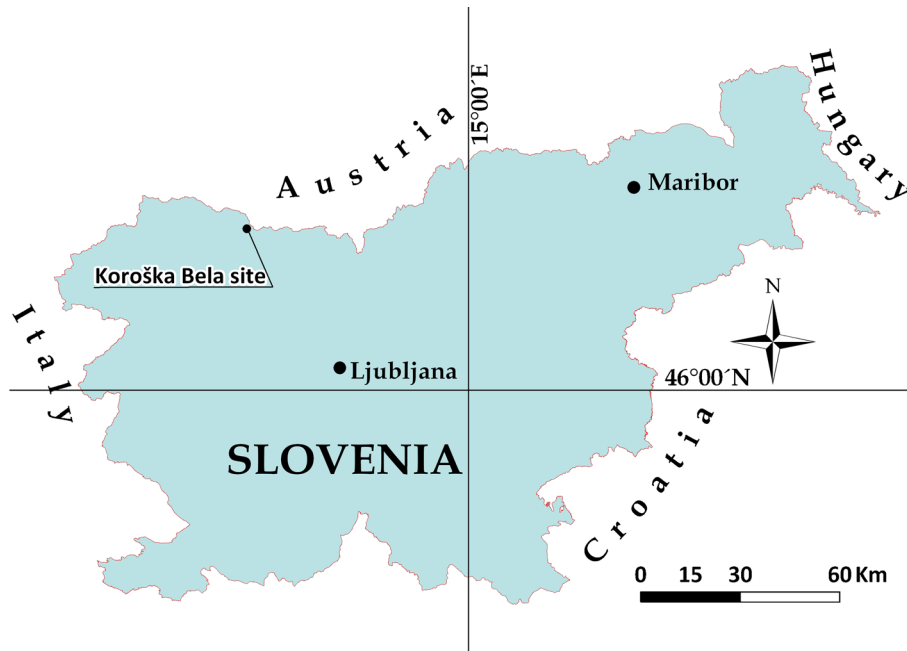
Fig. 1 Location of the studied landslide site Potoška planina is situated above the village of Koroška Bela, on the outskirts of the town of Jesenice in the Karavanke Mountain area of north-western Slovenia

The wider area is dissected by numerous faults linking the two major fault zones, Periadriatic and Sava fault zones. The underlying geology is composed of heavily deformed clastic (sandstone, siltstone and marlstone) and carbonate rocks (limestone and dolomite), with a large amount of talus material occurring in the upper part of the landslide at the foot of the ridge. Motion on the slide is predominately accelerated by percolation of surface and underground water, and the maximum volume of sliding masses has been estimated at about 1.8×10^6 m³ (Jež et al. 2008).

Meteorological data from 2004 to 2008 was obtained for a site approximately 1 km from Potoška planina and at a similar altitude (Planina pod Golico weather station). Meteorological data
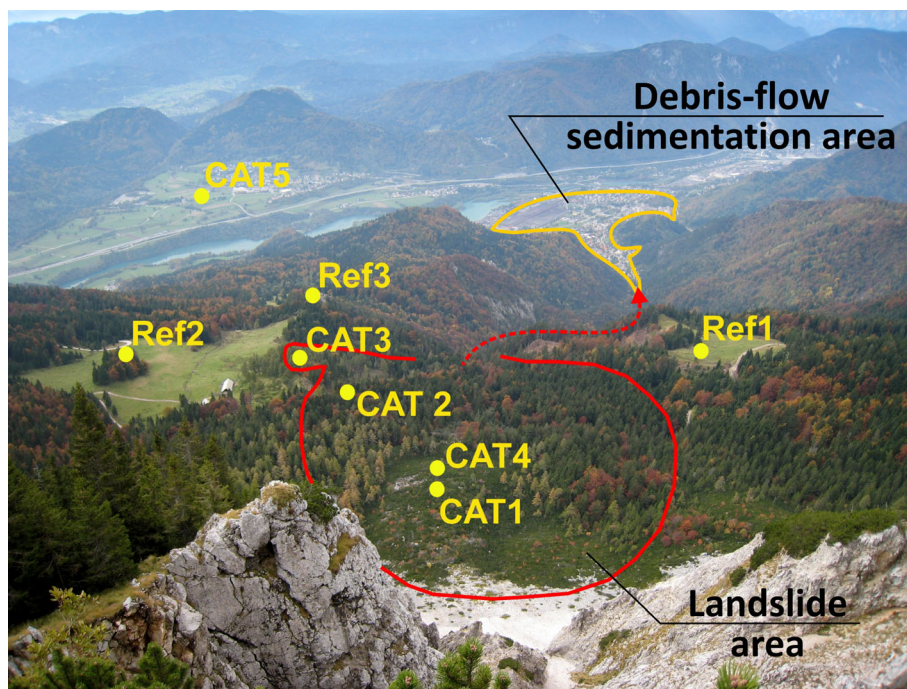

Fig. 2 View from the limestone ridge at the head of the Potoška Planina landslide, looking directly down the slide (*red*) into the ravine leading to the village of Koroška Bela (*yellow*). The Sava Fault runs along the valley below. The direction of the view is southwards. "CATx" represent the locations of the I²GPS units or solely CATs, and "Refx" represent the locations of the reference points

confirmed the reports from field observations that snow cover during the winter had the potential to cause interruptions to the service and that the units were likely to be operating within their temperature specifications for the majority, if not all, of the year. Both compact active transponder (CAT) and GNSS units suffer from phase artefacts if the antennae are covered by snow—for small amounts, it may be possible for snow to be cleared during field visits, but if more than 50 cm of snow would fall, this would not be possible and measurements would be invalid. Such snow clearance also relies on a field visit being practicable before each satellite overpass and on access to the site being clear. The meteorological data confirm observations that snow is likely from late November and may be heavy in January and February. However, the amount varies greatly from year to year, from almost none through to snow covers of several metres.

Unit locations

The ravine and lower area of the landslip are heavily forested, and therefore unsuitable for unit placement, but higher up the slope trees are smaller and there are several rocky areas which protrude from the trees. On both sides of the active slip lie areas of grassy pastoral land, which are assumed to be geologically stable and are ideal for reference point locations.

Test InSAR imagery was used to locate areas of the site where CATs would be visible and where they would be bright relative to the local background clutter. A further site was discounted for safety reasons due to its location on a steep rocky slope.

A total of three reference points (Ref1, Ref2 and Ref3) and four landslide points (CAT1, CAT2, CAT3 and CAT4) were selected for unit installation for the purpose of slope stability monitoring (Fig. 3). The main I2GPS reference point (Ref2) is located in an area of pastoral ground to the northwest of the landslip. Two further CAT reference points (Ref1 and Ref3) are located to the southeast and southwest, forming a triangle enclosing the lower half of the landslide. This configuration was designed to provide an estimate of a planar atmospheric gradient across the site. Intercomparison of the three points enabled evaluation of the stability of the main reference, and the additional references provided back-up in case the main reference failed or became unstable. There was an additional unit (CAT5) located on the south bank of the Sava river near the village of Blejska Dobrava (the distant area southwards, across the river on upper left part of Fig. 2), approximately 3.5 km from and approximately 600 m lower than the Potoška planina reference points for the purpose of monitoring active tectonics related to the Sava fault that runs along the valley. Measurement results from CAT5 are out of the scope of this paper and will not be discussed here.

Unit mountings were prepared in one of two ways, dependant on the local terrain. Where hard rock mounting points were available, a 3 cm hole was drilled and a metal post concreted in. Where the underlying ground was composed of soil or scree, a concrete foundation was constructed, with footings excavated approximately 0.5 m into the ground. This concrete was then drilled and a the post secured as before.

The metal posts are topped by a flat plate, with attachment points for the unit mounting and alignment structure. Each monument has an associated geodetic reference point marker, fixed firmly on the rock or concrete base structure. The mounting and alignment structure has been designed such that the phase centre of the GNSS antenna can be precisely centred over this marker at a known height offset. This ensures that points can be reliably re-surveyed at a later date even after unit removal, either by re-installation of the unit or surveying using conventional GNSS equipment.

Units were installed on the prepared monuments and accurately aligned. The base plate was levelled to within ±1° using a bi-axial spirit level and to within ±2° of true north using a compass. The GNSS antenna phase centre was precisely centred above the geodetic marker using a laser plumb. Positions of all units were initially surveyed with a handheld GNSS unit to provide location and topographic height estimates for use during SAR processing. Comprehensive instructions for installation and alignment were prepared within an operation manual provided to installation personnel. Unit locations were enclosed by a fence to reduce the risk of interference or damage from humans or animals.

Once in the field, units required regular visits for GNSS data to be downloaded for processing. The CAT units deployed could hold stored data and operational logs for several months of autonomous operation, but for the purpose of more timely access to the GNSS results for comparison with CAT processing and for closely monitoring the technical performance of the units, it was decided to visit the site on a monthly bases. In addition to GNSS positioning data, operation of both the GNSS and CAT units produces diagnostic and logging information to enable monitoring of unit function, and, alongside any deformation results, technical validation of the units was also a key outcome of the trial. Site visits also enabled checking the environmental conditions and mitigating any problems.

Methods

Persistent scatterers/InSAR and data processing

Persistent scattering technique is a technique that uses ground radar targets (persistent scatterers or PS) that through a longer period reflect (scatter) radar signal back to the satellite with a high reliability (signal coherence) (Ferretti et al. 2000; Hooper et al. 2004; Werner et al. 2003).

One of the major drawbacks of the technology is that it relies on natural or coincident man-made persistent scatterers that are already present on observed area and that the vegetation present hinders the ability of the method; artificial scatterers such as corner reflectors or compact active transponders (CATs) were developed (Crosetto et al. 2013).

Historically, the most commonly used wavelength for InSAR applications has been C-band with a wavelength of 5.6 cm, and hence CATs have been designed to operate at this band. We used them as a part of the unit in our study.

Two C-band instruments suitable for I2GPS-type projects are currently available or planned for launch (Table 1). Historically, the majority of InSAR work has utilised data from the two ERS satellites and the more recent Envisat operated by the European Space Agency (ESA). Of these, ERS-1, ERS-2 and Envisat are no longer in operation. Envisat ceased to operate in April 2012, although suitability for interferometry was reduced from October 2010.

Commercially, C-band data is available from the Canadian Space Agency (Can.SA) Radarsat-1 (MacDonald, Dettwiler and Associates Ltd. 2004) and Radarsat-2 (MacDonald, Dettwiler and
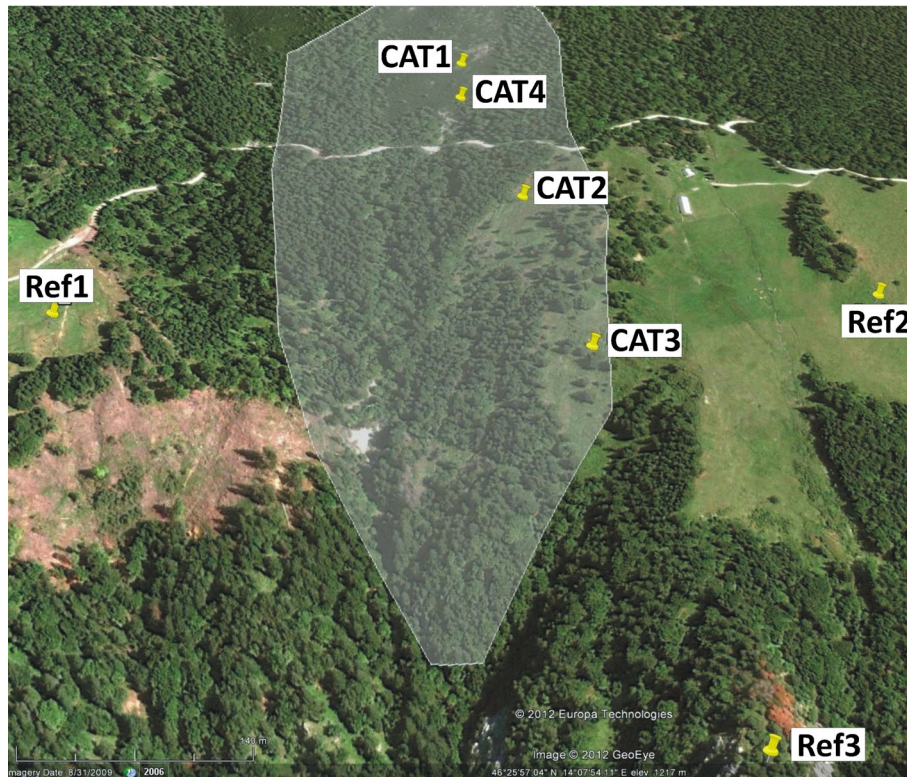
Fig. 3 Potoška planina site, showing approximate boundaries of slipping area (*shaded polygon*), and locations of CATs and Reference points (*yellow pins*). The direction of the view is northwards. Map image copyright Google, GeoEye 2006

Associates Ltd. 2011) satellites; however, data costs are an order of magnitude larger than for Envisat. In the longer term, ESA plan to launch SAR instruments aboard their Sentinel-1 satellites from 2014, these are expected to offer open access to data, potentially making operational I2GPS and similar projects more economical.

The designation C-band covers a range of frequencies. Previous CAT designs were optimised for frequencies of 5,300–5,331 MHz, used by the Envisat and Radarsat-1 satellites. The newer Radarsat-2 and Sentinel satellites moved to a frequency of 5,405 MHz to avoid frequencies being used for terrestrial wireless internet services. Unfortunately, this new frequency partially overlaps with the one used for air navigation, which places constraints on the CAT unit design and may, in some cases, complicate the radio transmission licencing that is needed to use CATs. Although the I2GPS field trials used Envisat data, new dual-frequency CATs were produced to demonstrate future compatibility with Radarsat-2 and Sentinel.

Satellites such as Radarsat and Envisat can be requested to acquire data over specific areas. Searchable catalogues are provided which describe a list of potential acquisitions; these can be selected and ordered, and are then programmed and uploaded to

the instrument by the satellite operator. Data are then delivered via FTP, usually within a few days of acquisition.

In some cases, conflict occurs when multiple users request data acquisition for an area using incompatible instrument modes, for example image mode (used for InSAR) and wide swath (WS), or request different incidence angles. There is also a period of un-availability when the instrument is required to change modes between successive imaging requests along the satellite track.

It is anticipated that the Sentinel-1 satellites will operate to a pre-defined acquisition plan, with a baseline target to achieve repeat coverage of all land areas every 12 days initially, and every 6 days once the second instrument is launched (ESA SP-1322/1 2012). Since data will be automatically acquired using a standard mode, programming will not be required and conflicts should be infrequent.

SAR data processing

SAR images were received from ESA via FTP download, within 3–5 days of image acquisition. Images were focussed and a single-look complex (SLC) image was produced. CAT units were identified, and their radar response measured at the point of peak

Table 1 Current and forthcoming C-band instruments suitable for I2GPS-type projects (MacDonald, Dettwiler and Associates Ltd. 2011; ESA SP-1322/1 2012)

Satellite	Operation body	Revisit time (day)	Incidence angle	Resolution (m)
Radarsat-2	MDA	24	10–60	1.6–26
Sentinel-1	ESA	6–12	20–47	1.6–160

amplitude. The left part of Fig. 4 shows a section of the of radar image (displayed in radar geometry not in a map projection; the image is of the order of 100 m across) from an ideal case, and the right part of Fig. 4 shows the cross-sections along the white lines on the left image. The vertical scale on the graphs represents uncalibrated image intensity and is displayed in arbitrary units. Both figures are a general example of an artificial reflector and were not acquired during the trial presented in the paper. Two SLC images were then co-registered using a combination of knowledge of the orbital geometry and image cross-correlation, and combined to form a complex interferogram. Phase contributions from orbital and topographic effects were modelled using details of the orbital geometry combined with a digital elevation model (DEM), and subtracted from the interferogram.

Where sufficient coherence was present in the wider area surrounding a site, estimation of residual orbital and large-scale atmospheric trends was possible. These trends were modelled based on a planar gradient, and subtracted from the interferogram (Fig. 5). Phase values for each CAT were then extracted from the interferogram.

Extracted phase values were considered relative to a selected CAT chosen as a fixed reference point. The reference point phase was subtracted from each remaining CAT measurement to give a phase difference. Phase measurements (ϕ, in radians) were then scaled to represent apparent line-of-sight (LOS) deformation (D_{LOS}) in millimetres, using Eq. (1), where 28 mm represents the half of the wavelength of the radar signal:

$$D_{LOS} = \frac{28}{2\pi} \cdot \phi \tag{1}$$

Phase measurements were recorded modulo 2π, due to the cyclic nature of phase (Fig. 6), resulting in potential for ambiguities in motion measurements. In conventional DifSAR processing, these ambiguities can usually be resolved by using an assumption of smooth spatial variation to identify and compensate the anomalous phase jumps (termed 'unwrapping') (Ghiglia and Pritt 1998). However, this is more challenging for point measurements, where there are no intervening phase measurements to identify phase jumps between points.

Initially, these phase ambiguities were resolved using an assumption of minimal motion over the time span of the interferogram (Fig. 7); however, these estimates could later be revised in the context of spatial and temporal information for the site or GNSS motion information where available. Estimates of uncertainty in the phase measurements were calculated from an examination of the local background clutter conditions (Ketelaar et al. 2004).

Processing of the results was performed in the PULSAR interferometry software (http://www.phoenixsystems.co.uk/). Topographic phase was a significant factor for the point scatterers due to the large variations in topographic relief; this was calculated using heights derived from GNSS measurements. Orbital phase trends were estimated and removed from interferograms which contained sufficient coherence based on visible phase gradients.

Data acquisition utilised data from ESA's Envisat satellite. ESA announced that there would be changes to the orbit of Envisat beginning in October 2010. Although a few scenes were acquired before the change, the majority of the trial data were acquired from February 2011 onward. It was widely reported that data acquired after the Envisat orbit change would undergo a progressive lengthening of baselines with respect to the start of the mission phase as orbital inclination was allowed to drift (Miranda et al. 2009). It was anticipated that this would limit interferogram timespans to relatively short-term pairs. While an increase of baselines was observed, this was not as severe as initially expected, and interferometry remained possible between the first and last SAR images. However, the orbital change did restrict useful acquisitions to descending data, preventing estimation of horizontal and vertical motion using two lines of sight.

Programmed acquisitions before and after the orbit change were affected by numerous scheduling conflicts and cancellations, making collection of a continuous time series difficult. After
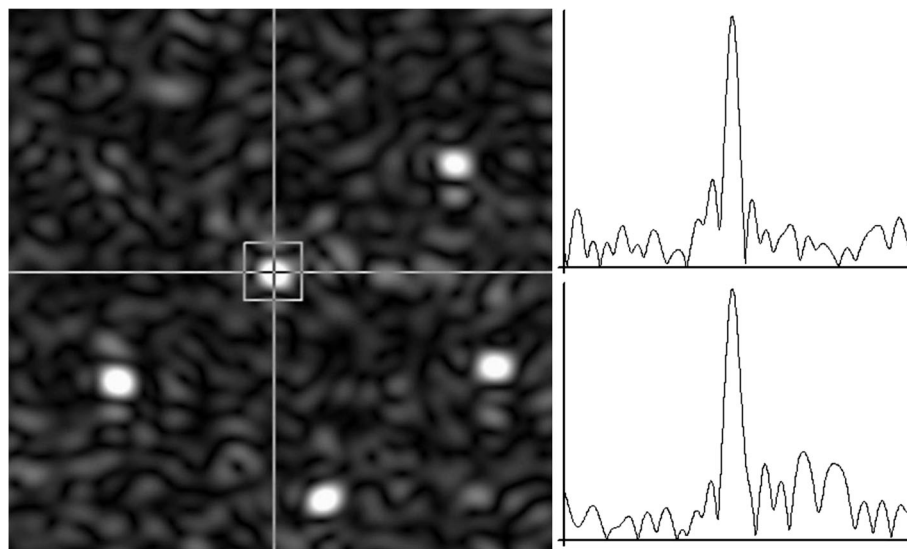

Fig. 4 An ideal case of the identification of CAT response in SLC image (*left*), displayed in radar geometry (not in a map projection) with the order of 100 m across, and two cross-sections (right) along the *white lines on the left image*. The *vertical scale on the graphs* represents uncalibrated image intensity (showing the response as a function of range and azimuth) and is displayed in arbitrary units measurement
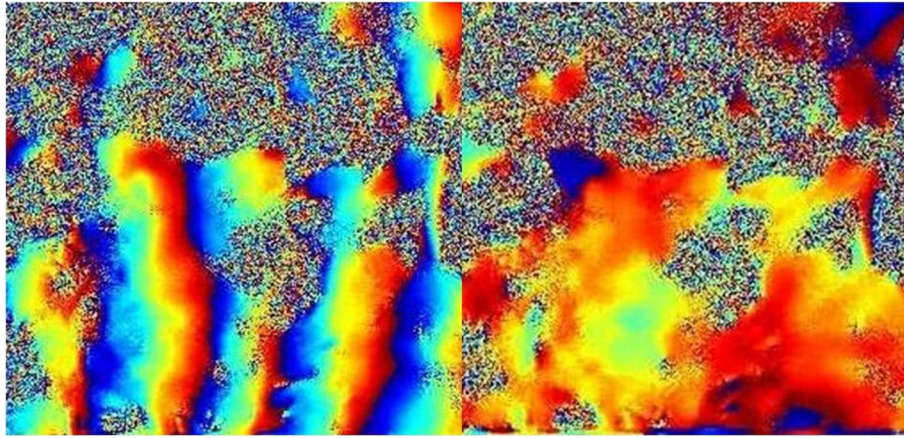
Fig. 5 Section of wrapped interferogram showing a strong residual orbital trend due to poor-quality orbital state vectors (*left*), and the same area after removal of a planar phase gradient (*right*)

helpful discussion with ESA, it was confirmed that many of these clashes involved the European Maritime Safety Agency (EMSA), who acquire SAR data for their 'Clean Sea Net' maritime monitoring programme in the northern Adriatic. EMSA were exceedingly helpful in working with partners in the project I2GPS responsible for SAR imagery acquirement, finding a solution to the conflicts and agreeing to avoid programming on the desired I2GPS tracks for the duration of the trial. No further conflicts were encountered during trial data collection.

Initial SAR images encountered problems with CAT visibility. A systematic review of potential causes was undertaken with an estimation of likelihood, and relevant diagnostic procedures were outlined for each factor. The majority of these were eliminated by checks on the SAR data and processing, field observations and functional checks of the units. Once Envisat data collection

Fig. 6 The observed phase difference due to increasing LOS displacement (*red arrows*) increases until the phase offset is equal to a complete wavelength (here equivalent to 28 mm of deformation). At this point, the offset phase is identical to the original phase, and no deformation appears to have occurred

resumed, it was determined that the main cause of the visibility loss was the restriction on CAT beam width. Although designed to provide a maximum effective radar cross-section (RCS) of 32 dB m^2, this declines away from boresight (35°), and at the steep local incidence angle of the initial SAR observations (~20°) the resulting RCS was too low to unambiguously identify the CATs against background clutter.

The data acquisition plan was modified to use a primary track acquired at a shallower angle (IS3, ~29° local incidence angle), which improved CAT visibility. A second IS2 'backup' track was acquired (381, not listed in Table 2) for use in the event that the optimal track suffered from cancellations, this track was slightly steeper and did suffer from some residual visibility problems, degrading the quality of results from this track. As such, interpretation of results focused primarily on the primary track 108, where result quality is higher. Table 2 lists the post-orbit-change SAR scenes acquired across the site for track 108.
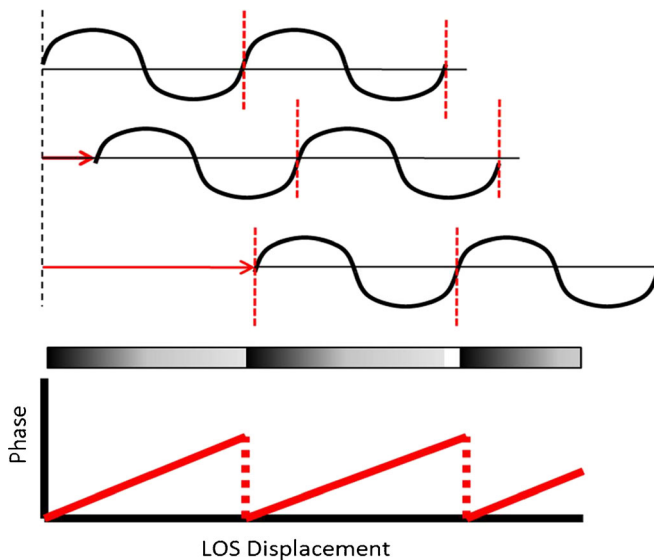
GPS/GNSS data processing

The GPS data was collected by the I2GPS units on a continuous basis. The GPS observations were stored with a 30-s sample rate. A new file was started each day by the receiver and the files were downloaded at regular intervals from the receiver (once every 1–2 months) using a laptop and USB connection to the receiver.

The GNSS processing consisted of two main steps: (1) data pre-processing and (ii) GPS solution using the Bernese GPS Software version 5.0 (BSW50) (Dach et al. 2007), following all standards set for the IGS and European Reference Frame (EUREF) processing (Dow et al. 2009; Bruyninx 2004). During pre-processing, data logged in the receiver's proprietary format (Septentrio Binary Format) was converted into the Receiver Independent Exchange Format (RINEX Version 2.11) using Septentrio's *sbf2rin* and the quality of the data was checked using *teqc* from Unavco. Plots of the data quality checking have been generated using *Matlab* tool.

In Fig. 8, an example of the information that can be found in the summary files is given for CAT1 (GPS code KBC1), CAT3 (GPS code KBC3), CAT5 (GPS code KBC5) and Ref2 (GPS code KBR2) locations, showing the percentage of daily data that is tracked (stored). Other performance indicators are the number of satellites that are tracked, the number and percentage of observations
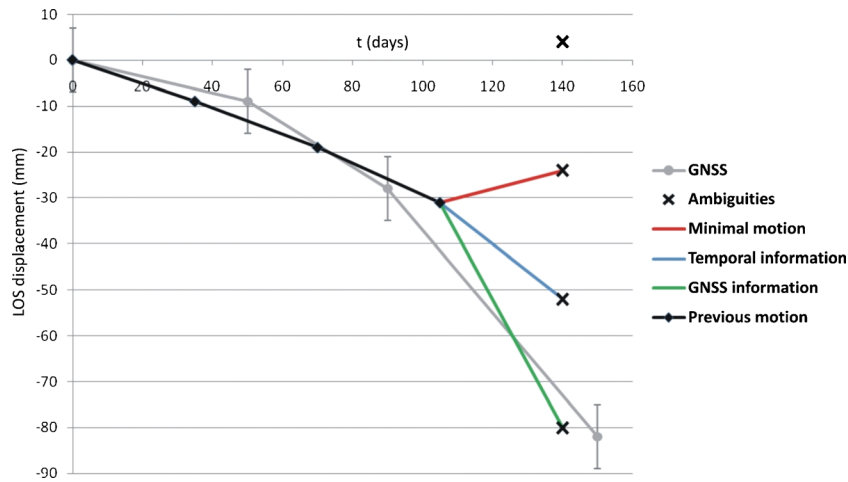
Fig. 7 Plot of hypothetical deformation measurements from a CAT unit (*black line*), with black crosses marking the latest measurement modulo 2π. Possible assumptions to resolve the ambiguity could include minimal deformation (*red*), trend from previous measurements (*blue*) or closest fit to GNSS data (*green*)

(above the horizon and above 10° elevation) and the pseudo-range noise statistics. The example in Fig. 8 clearly shows the tracking problems during the winter period due to the power deficit of the solar panels caused either by cold or snow cover.

The RINEX files store the raw pseudo-range and carrier phase data for the satellites tracked by the receiver. The receiver does not output any position information other than a rough pseudo-range solution. It should be noted that the receiver does not do a real-time kinematic (RTK) solution, as this does not provide the desired level of precision in the solution for deformation studies. Instead, the raw pseudo-range and, in particular, the carrier phase data is later post-processed to obtain the precise location of the receiver antenna. This was the second phase of the GNSS processing.

The main GNSS processing consisted of a GNSS ionosphere-free network solution using the BSW50 software (Dach et al. 2007), following the standards set for IGS and EUREF analysis centres (Dow et al. 2009; Bruyninx 2004). The network of four I2GPS stations was therefore extended with seven IGS Permanent GPS stations with highly accurate station coordinates and velocities in the International Terrestrial Reference Frame 2008 (ITRF2008). These stations provided the reference frame for the four I2GPS stations. A GPS permanent station in Ljubljana was added to the network in order to have another reference station in the network, which is to be processed in exactly the same way as the four I2GPS

stations, and that can be used for comparison purposes and as additional stable point.

The main goals of this processing step were (1) to obtain the best possible site coordinates and position time series in a global reference frame (ITRF2008), (2) to obtain estimates of the atmospheric delay (Tropospheric Zenith Delay) over the area of interest and (3) to verify the stability of the presumed stable reference points (KBR2/Ref2).

The Bernese software computes an unconstrained-free network solution that does not initially use any coordinate constraints for the IGS stations. This allowed us to verify the stability of the reference stations. The free network solution was in a final step linked to the absolute reference frame by a three-parameter Helmert transformation (shifts in X, Y and Z) making the closest possible fit of the IGS stations onto the values given in the ITRF2008 reference frame (using station coordinates and velocities from the IGS08 realisation of the ITRF2008 reference frame). It should be pointed out that the external coordinates for the IGS stations were only used to determine a shift from the free network solution onto the absolute reference frame.

The I2GPS antenna type, called SATIMO-005-A, was unknown within IGS/EPN. Therefore, before the processing commenced, absolute antenna calibrations, as measured by Satimo, have been introduced into the antenna calibration files of the Bernese GPS software. This was a very critical step in setting up the processing

Table 2 SAR images across the Potoška planina site acquired after the Envisat orbital change

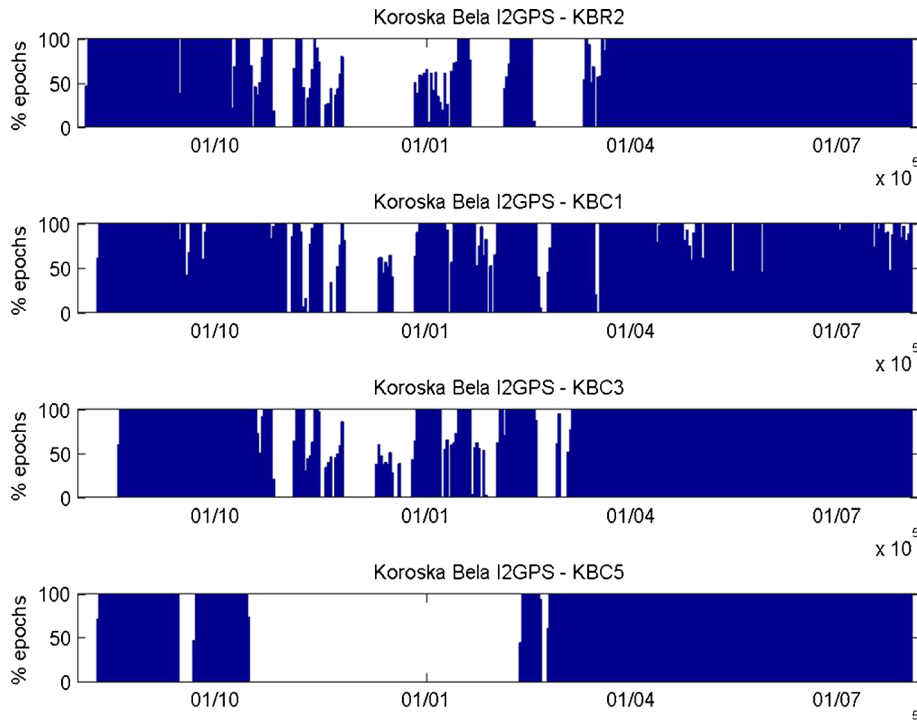| Acquisition date	Time	Track	Model	Local incidence angle
02/02/2011	09:22	108	IS3	28.8
04/03/2011	09:22	108	IS3	28.8
03/04/2011	09:23	108	IS3	28.8
03/05/2011	09:23	108	IS3	28.8
02/06/2011	09:24	108	IS3	28.8
01/08/2011	09:25	108	IS3	28.8

Fig. 8 Example of a data quality plot generated during preprocessing. KBR2 is a GPS coding for Ref2; KBC1 is a GPS coding for CAT1; KBC3 is a GPS coding for CAT3; KBC5 is a GPS coding for CAT5 (not elaborated in this paper)

for new equipment and a potential area of mistakes, especially with a new provider of antenna calibration values (Satimo).

The resulting solution is saved in the Solution Independent Exchange (SINEX) format, which included the station coordinates and the full co-variance matrix of the solution, as well as the estimated tropospheric zenith delays (as separate files), that are used for the integrated processing.

Integrated data analysis (co-registration of InSAR and GPS/GNSS data)
The main goal of the project I2GPS was to develop an integrated system that would allow continuous GPS/GNSS and InSAR co-registered data collection, and, for that purpose, an I2GPS unit was compiled. Once InSAR and GPS/GNSS data acquired by the unit have been processed, a cross-comparison of the two datasets was performed. InSAR data produced relative LOS motion measurements with respect to a reference point (Ref2). In order to compare motion measurements from the GPS/GNSS data, these had to be projected into the satellite LOS to calculate the equivalent component of the 3D GPS/GNSS motion vector. Initial assumptions about InSAR measurement ambiguities were revised in light of motion information from the GNSS, since the precision of the GPS/GNSS measurements is expected to be sufficient to resolve these ambiguities. Then, the degree of correspondence between the two was examined.

There are possible benefits of the integrated processing of the GPS/GNSS and InSAR data and these are: (1) an integrated 3D displacements in the absolute International Terrestrial Reference Frame, (2) atmospheric correction of the InSAR data using estimated GPS zenith delays and (3) ambiguity resolution for InSAR data over longer baselines.

In order to fully exploit all possible benefits of the I2GPS unit for the purpose of the 3D displacement monitoring, there has to be a fixed relation between the phase centres of the GPS/GNSS and CAT of the I2GPS unit, and this relation must not change in time in order to successfully integrate of the two measurements sets. The design of the I2GPS units is sufficient guarantee that this condition is met. Even when a unit is reinstalled, or replaced by another unit, the condition is still fulfilled through the alignment facilities and procedures that are part of I2GPS unit and installation procedure. The benefit of integrated units (I2GPS) is that it is easy to maintain a fixed relation between InSAR and GPS, and that this relation can be repeated after a remount. It is also possible to obtain 3D displacement vectors for the I2GPS units, but the first condition has to be met (an integrated GPS/GNSS and InSAR unit or system). Integrating GPS/GNSS with InSAR, gives, from the InSAR perspective, 3D displacements. Vice versa, integrating InSAR with GPS/GNSS gives improved estimates in the height component and refines the velocity estimate of the GPS/GNSS system. This procedure is based on an integrated adjustment of the 3D GPS displacements, at the epoch of a SAR acquisition, with the full co-variance matrix as computed by the GPS processing together with the line-of-sight displacements from InSAR with the co-variance matrix from the SAR processing.

The differential phase measured for CAT units contained a component from variations in atmospheric refractivity across the site. To minimise this source of error, constraints were placed on the distance and change in elevation between each unit and the reference points. GPS/GNSS processing may also include generation of an estimate of the TZD encountered by electromagnetic radiation travelling between the satellite and the ground due to atmospheric refractivity. These calculated delays could be used to

estimate the differential LOS delay corresponding to InSAR measurements, which could then be subtracted to give corrected results. TZD corrections were produced as part of the tectonic element of the field trial (related to CAT5); however, these results are beyond the scope of this paper.

InSAR gives displacements in the line of sight with respect to a reference epoch. With GPS, we obtain displacements in three dimensions in an "absolute" reference frame. The reference frame used for GPS in this campaign is the International Terrestrial Reference Frame ITRF2008 which is maintained by the International Association of Geodesy (IAG) by means of various observational techniques (GPS, SLR, VLBI). Two immediate benefits of integrating InSAR with GPS are: (1) displacements in an absolute reference frame for all CAT and I2GPS units, as long as there is one I2GPS unit in the network, and (2) improved 3D displacement vectors for all I2GPS units in the network.

If there is at least one I2GPS unit in the network, the displacements from all CATs and other persistent scatterers can be computed in the International Terrestrial Reference Frame. The operation is fairly straightforward—if there is only one I2GPS unit in the campaign, and assuming this unit has been used as a reference (e.g. KBR2/REF2), the GPS displacements in the line of sight simply have to be added to the InSAR displacements (obtained with respect to the reference unit). If there are multiple I2GPS units in the campaign, then the combination can be done through a simple adjustment.

Results and discussion

InSAR results and discussion

Approximate uncertainties for each CAT measurement were calculated based on the RCS of the response compared to the magnitude of surrounding clutter (Table 3). They represent an estimate of the accuracy with which the actual CAT response phase can be measured from the SAR image in terms of contamination from background clutter. For a given brightness of background, the weaker the CAT signal the greater the proportion of that phase measurement is coming from elsewhere and the higher the resulting uncertainty. There may also be additional uncertainties introduced through other effects related to low magnitude responses, for example misestimation of the location of peak amplitude; however, these effects are harder to quantify. In addition, the estimated uncertainties do not include sources of error which stem from external contributions to measured interferogram phase, for

example orbital and atmospheric components. The average uncertainty estimate for track 108 was ±1.28 mm, not accounting for Ref2 as it is the main I2GPS reference.

CAT responses were derived using a 'single master' approach, measuring deformation in each SAR image relative to the first date, minimising errors due to phase estimation from the SAR images. As an additional check, further 'short-timespan' interferograms were produced between adjacent SAR images; these are usually more coherent so trend estimation is more reliable; however, phase measurement and orbital estimation errors add cumulatively along the time series making the later measurements less accurate. The single master interferogram measurement for a given epoch should have coincided with the cumulative sum of the short-timespan interferograms to within the estimated uncertainties. Where this was not the case, residual differences were likely to stem from variations in orbital phase corrections applied to the various interferograms.

Since Ref3 did not have stable phase, it was not possible to use the three reference points to estimate and remove a local phase gradient due to atmospheric and orbital sources. Orbital phase trends were instead estimated and removed from interferograms which contained sufficient coherence based on visible phase gradients.

The CATInSAR results were measured in the descending LOS direction, so negative displacements (away from the satellite) could include elements of both downward and westward motion, and positive displacements could include upward and/or eastward motion (Table 4).

The interferogram-wide estimation of orbital trends does not remove smaller-scale components of atmospheric phase variation, but these were expected to be small for all CATs (relative to Ref2) due to the small size of the Potoška planina site and hence small distances between observed locations and Ref2 (Crosetto et al. 2013).

The large-scale phase variations seen at Ref3 (Fig. 9) are believed to stem from phase contamination from adjacent bright pixels, rather than ground motion. This risk was foreseen during trial planning and test SAR data was acquired in order to avoid areas of background scatter. However, the positioning accuracy of this assessment was limited by the coarse resolution of available DEM data used to geocode the SAR image. One of the purposes of the post-installation visibility check was also to detect such a problem and apply any necessary correction before the full trial started. Unfortunately, other visibility problems

Table 3 Estimated uncertainty (mm) at each location, relative to Ref2 and 2nd of Feb, for CATPSI results for track 108 SAR data presented in Table 4

Acq. date	2 Feb 2011	4 Mar 2011	3 Apr 2011	3 May 2011	2 Jun 2011	1 Aug 2011
Ref1	0.00	1.28	1.33	1.24	1.13	1.26
Ref2	0.00	0.00	0.00	0.00	0.00	0.00
Ref3	0.00	1.30	1.18	1.13	1.09	1.14
CAT1	0.00	1.35	1.23	1.31	1.26	1.26
CAT2	0.00	1.00	4.64	1.13	1.14	1.09
CAT3	0.00	1.03	0.92	0.97	0.88	1.11
CAT4	0.00	1.32	1.28	1.26	1.13	1.19

Table 4 Cumulative deformation (mm) at each location, relative to Ref2 and 2nd of Feb, derived from Track 108 SAR data

Acq. date	2 Feb 2011	4 Mar 2011	3 Apr 2011	3 May 2011	2 Jun 2011	1 Aug 2011
Ref1	0.0	−1.57	−2.35	−2.83	−2.45	0.18
Ref2	0.0	0.00	0.00	0.00	0.00	0.00
Ref3	0.0	7.95	4.42	−2.90	4.86	−6.97
CAT1	0.0	−1.77	−7.39	−10.15	−13.38	−14.56
CAT2	0.0	−1.08	−8.70	−8.88	−8.65	−4.73
CAT3	0.0	−0.52	1.58	−0.98	−2.01	1.72
CAT4	0.0	−0.29	−6.51	−9.59	−9.95	−12.35

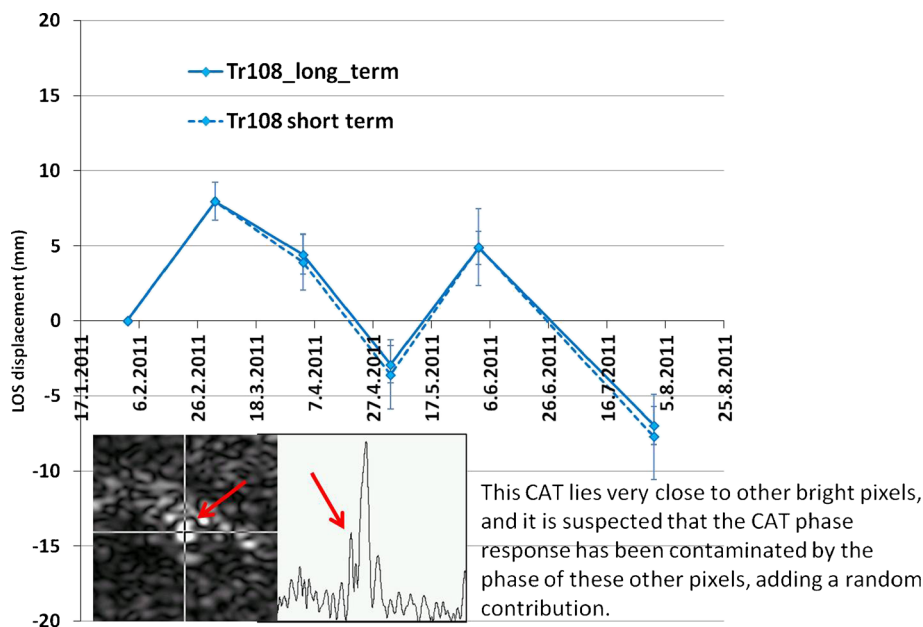meant that the problem did not become apparent until well into the trial.

Figure 10 shows the InSAR and GPS/GNSS motion measurements for CAT1 (above) and CAT3 (below) projected into track 108 LOS. While for the CAT1, the measurements are coherent (both moving away from the satellite, t.i. downwards), this cannot be stated with certainty for CAT3 as, here, the measurements are appearing to be contradictory (while one moves away from the satellite, the other moves towards and vice versa). Still, the differences in GPS/GNSS and InSAR measurements at CAT3 are only marginally larger than the uncertainties; hence, it is possible that observed displacements are not that different. Nevertheless, the assumption of minimal motion used to reconcile the InSAR motion ambiguities appears to be realistic, and it is considered unlikely that high motion rates are causing ambiguity limits to be exceeded in any epoch.

GPS/GNSS results and discussion

The quality of the GPS solution can be expressed in several ways. The formal standard deviation in the north and east is generally below 0.5 mm, while the standard deviation for the height is between 1.5 and 2 mm. The Chi^2/df (degree of freedom) test statistic for the daily solutions is between 1.1 and 2.9, with expected value of 1. This corresponds to a standard deviation of the carrier phase observations between 1.05 and 1.7 mm. The Chi^2/df statistic was significantly lower during the winter period than during the summer. This is not unusual as this is often related to residual atmospheric delays, but it could also be partly explained by the fact that during the winter period the Potoška planina receivers were experiencing tracking problems and hence were not present in calculations of the winter solutions. It is well known that the formal standard deviations are on the optimistic side, as these standard deviations, like the Chi^2 statistic, only represent the internal accuracy during the daily processing. In particular, the formal standard deviations ignore the effect of long periodic and systematic orbit errors.

Instead of the formal standard deviations, one can consider the daily station repeatability as an indicator of the quality of the solution. The average of daily station repeatability for seven reference (IGS) stations in the LOS was 3.2 mm, while the average daily repeatability for Potoška planina receivers was 5.1 mm. The daily station repeatability is defined as the root mean square error of the

This CAT lies very close to other bright pixels, and it is suspected that the CAT phase response has been contaminated by the phase of these other pixels, adding a random contribution.

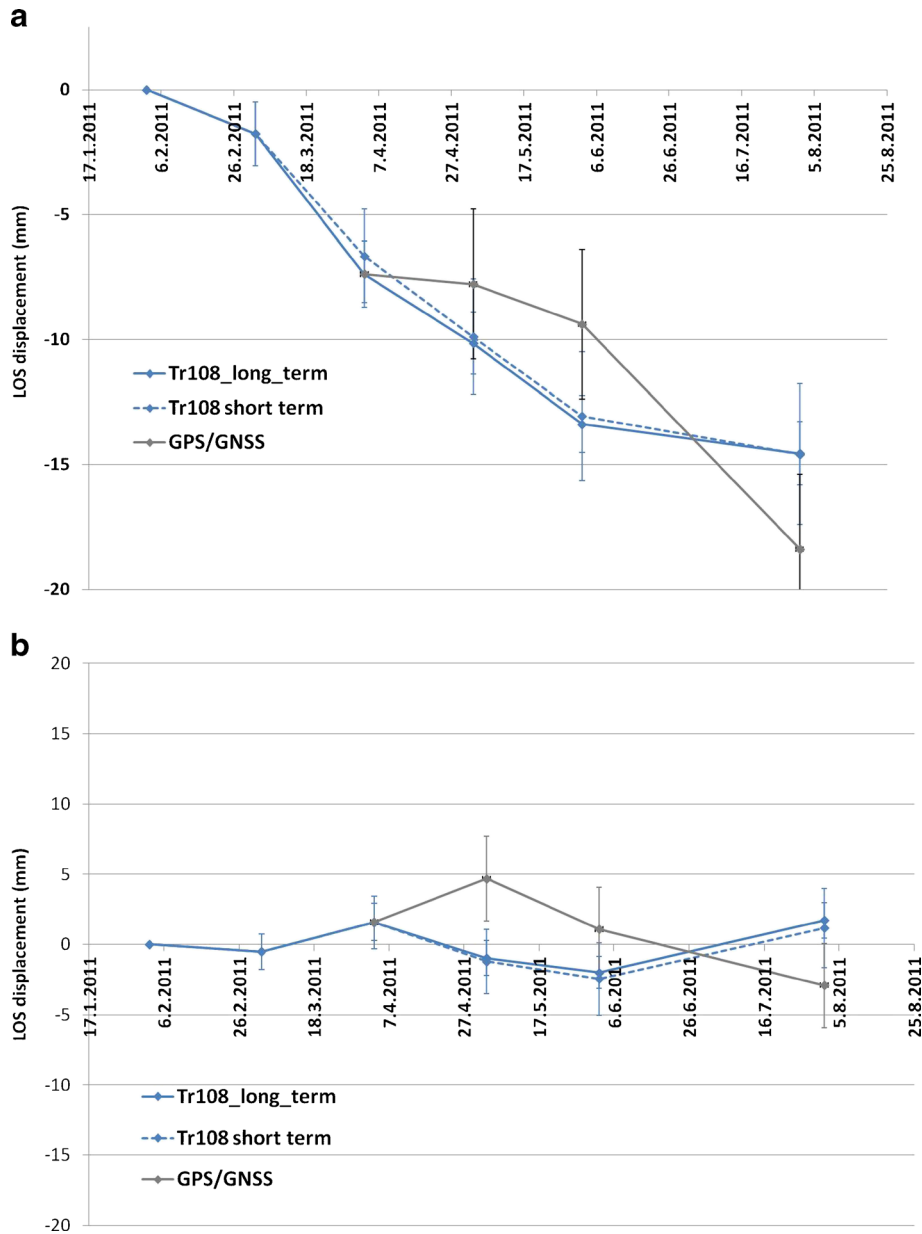**Fig. 9** Example of scale phase measurements at Ref3

Fig. 10 LOS displacement measurements for CAT1 (*above*) and CAT3 (*below*) relative to Ref_2

daily station coordinates after fitting a linear trend to the coordinates. These repeatabilities therefore contain two error contributions—(1) the estimation error of the GNSS processing (true error, including all possible effects) and (2) an effect of residual station motion (all motions that cannot be described by a linear trend). Compared to the formal errors, which tend to be too optimistic, the repeatabilities are over bounding the GNSS errors and are on the pessimistic side.

The daily station repeatability is about twice as large as the formal standard deviations—it is about 1–1.5 mm for the north and east components and 3–3.5 mm for the height of the IGS stations. For the Potoška planina stations, the repeatability is larger—for the north and east about 2–3 mm and for the height, it is 5–7 mm. This could be related to the GPS receiver and antenna for the I2GPS units (tracking problems due to power interruptions,

new and unknown antenna type, setup with metallic baseplate) or residual motion of the units (within the day) due to the deployment on an instable area. Another effect could be snow on the antenna (snow on the GPS antenna will introduce significant errors). In the computation of the repeatability, we have not done any outlier rejection. If we remove the partially observed days and other outliers, the repeatability are slightly improved. Given the fact that the best achieved repeatability at IGS stations was 2.8 mm in the LOS, we can conclude that the GNSS accuracy in the LOS for Potoška planina locations would be around 3 mm (standard deviation).

In Fig. 11, the time series in north, east and up coordinates for Ref2 is given corrected for the known plate motion from the Nuvel-1A model. In Figs. 12 and 13, the time series in north, east and up coordinates for CAT1 (KBC1) and CAT3 (KBC3) are given
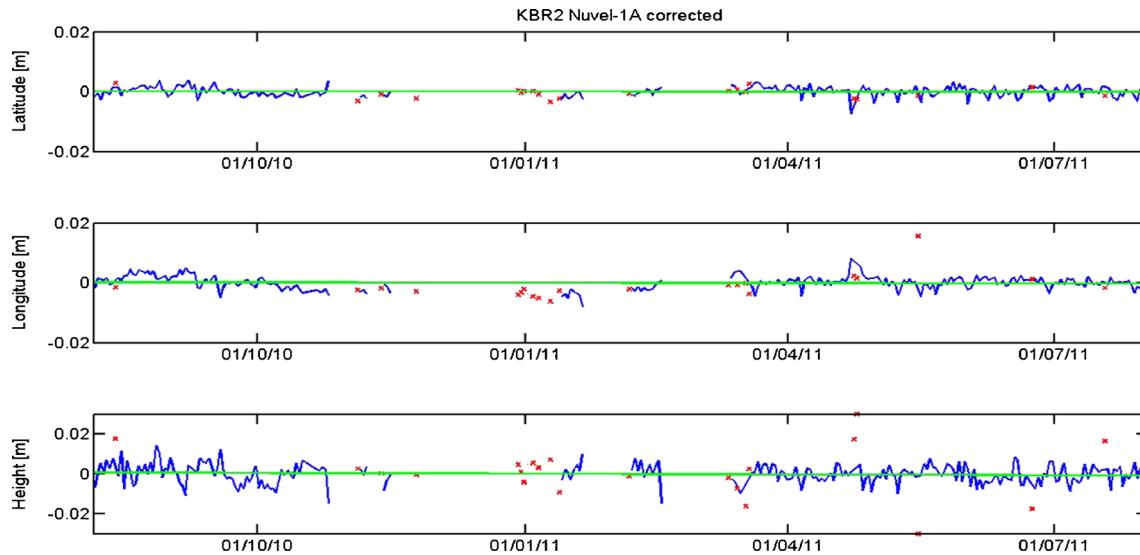
Fig. 11 Time series in north, east and up for REF2 (KBR2) in IGS08 (ITRF2008) corrected for Nuvel-1A plate motion. The *green line* is the fitted trend line. The *red crosses* are GPS samples where the receiver did not track the GPS signals for more than 16 h/day

respectively with respect to the Ref2 (KBR2). The coordinates were computed in the IGS08 (ITRF2008) reference frame, and the known motion for the Eurasian plate from the Nuvel-1A model has been subtracted from the coordinates (−0.0144, 0.0180 and 0.0092 m/year in the X, Y and Z direction). At the end time series for Ref2 were subtracted from time series of CAT1 and CAT3 to get their relative rates (vectors) of movement. Represented values are actually the coordinate differences CAT1-Ref2, CAT3-Ref2, which represent coordinate vectors or baselines, from Ref2 to CAT1 and CAT3, respectively. The green line in Figs. 12 and 13 is the fitted trend line. The red crosses are GPS samples where one of the receivers (either the reference receiver Ref2, or target receiver CAT1 or CAT3) tracked the GPS signals for less than 16 h/day. The repeatability was computed after subtracting the linear

motion. If no data for Ref2 was available, also no results for the baselines to CAT1 and CAT3 were available. It is therefore rather disturbing that Ref2 had a lot of tracking problems during Feb/March 2011 as shown in Fig. 8.

The estimated average rates for these stations (after correction for Nuvel-1A plate motion and in relation to Ref2) and station repeatability are given in Table 5. The repeatability is computed after subtracting the yearly velocity. Still we have to be careful with interpretations as motions may not always be linear and this may affect the repeatabilities (computed after removing the linear motion). Also the period of data collecting was too short for estimation of other motions than a linear motion although the GPS/GNSS data plots (Figs. 12 and 13) indicate at some evidence for non-linear motions.
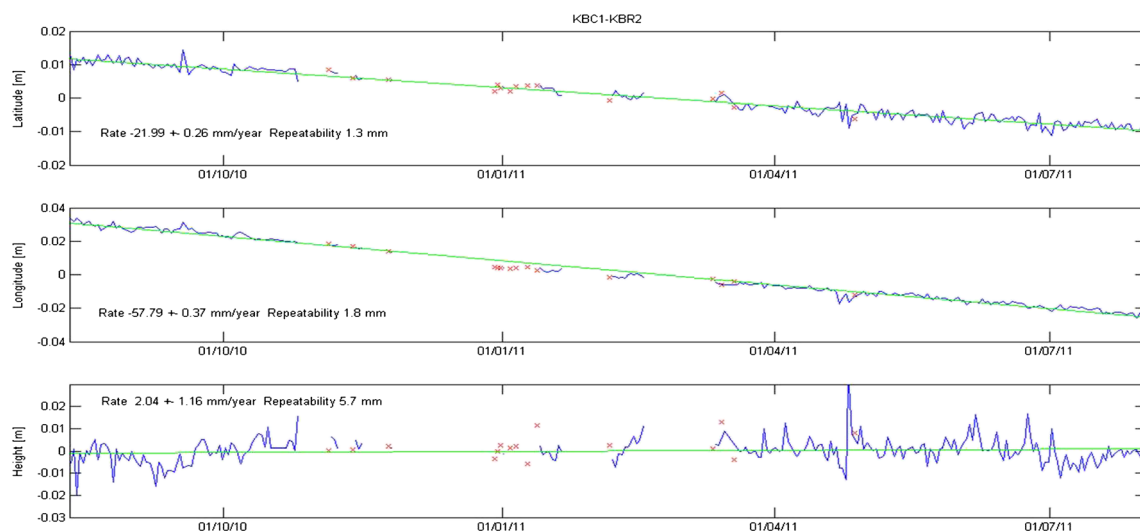

Fig. 12 Time series in north, east and up for CAT1 in IGS08 (ITRF2008) corrected for Nuvel-1A plate motion and in relation to the Ref2. The *green line* is the fitted trend line. The *red crosses* are GPS samples where the receiver did not track the GPS signals for more than 16 h/day

Fig. 13 Time series in north, east and up for CAT3 in IGS08 (ITRF2008) corrected for Nuvel-1A plate motion and in relation to the Ref2. The *green line* is the fitted trend line. The *red crosses* are GPS samples where the receiver did not track the GPS signals for more than 16 h/day
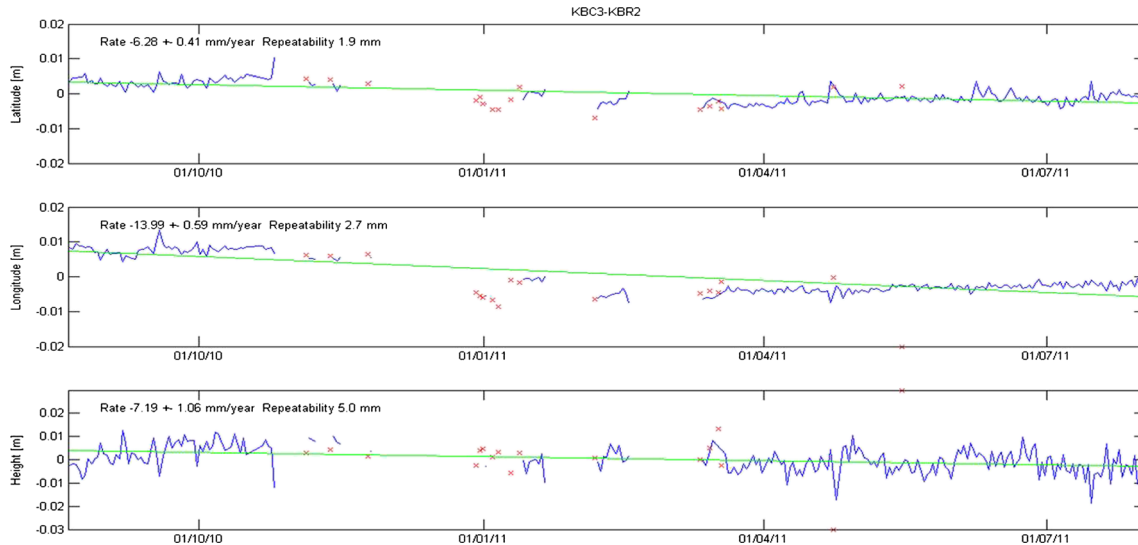
When calculating absolute rates of stations' movement also, data from the nearby EPN station GSR1 (Ljubljana, Slovenia; see Table 5) was included and it was treated in a similar way as the four I2GPS stations Ref2, CAT1, CAT3 and CAT5. This was done for comparison purposes, and to have another alternative for a stable (non-moving) marker. Results show that Ref2 is suitable as a stable reference point.

If we compare the results of the baselines (last three rows in Table 5) to the repeatabilities in an absolute frame (first four rows in Table 5), we can observe that the north and east repeatabilities for the short baselines CAT1'=CAT1−Ref2 and CAT3'=CAT3−Ref2 are improved. The up repeatability is about the same for these two baselines. An improvement in results is quite important as it implies that by taking differences between stations some common mode error has been removed. If the data would have been uncorrelated, then we would have expected an increase in the repeatability by a factor of 1.4.

Results of integrated GPS/GNSS and InSAR data analysis and discussion
A comparison of the two measurement datasets is possible if the displacements from GPS/GNSS are plotted in the same system

(Fig. 14). The cyan line with crosses is the LOS deformation for GPS/GNSS; it is the LOS deformation difference with the reference Ref2. It has been computed by projecting the displacements at CATs onto the line of sight to the SAR satellite. The red crosses are GPS/GNSS samples where the receiver did not track the GPS/GNSS signal for more than 16 h/day. The green line is the fitted trend line and the magenta curve is the 7-day running average of the GPS/GNSS. The GPS/GNSS repeatability that is reported is computed after subtracting the trend line.

The displacements from InSAR are shown in Fig. 14 as black diamonds and stars. The diamonds are the InSAR displacements computed from using a single master image (long-term displacements); the stars are the InSAR displacements resulting from the cumulative summing of consecutive pairs of images (short-term displacements).

Figure 14 represents difference between receiver single differences displacements of the GPS with respect to a certain reference epoch. The reference epoch is not the same at the reference epoch for the InSAR double difference (temporal and spatial) displacements. The InSAR double difference displacements have been aligned to the GPS double difference displacements by shifting the InSAR data such that the difference between the GPS and

Table 5 Estimated velocities for GSR1, Ref2, CAT1 and CAT3 in millimetre per year in IGS08 corrected for Nuvel-1A plate motion, estimated velocities for Ref2', CAT1' and CAT3' in millimetre per year with respect to the Ref2 (Vel N, Vel E, Vel Up—velocity towards N, E and Up, respectively) and daily repeatabilities (after subtracting the linear motion) in millimetres (Rep N, Rep E, Rep Up)

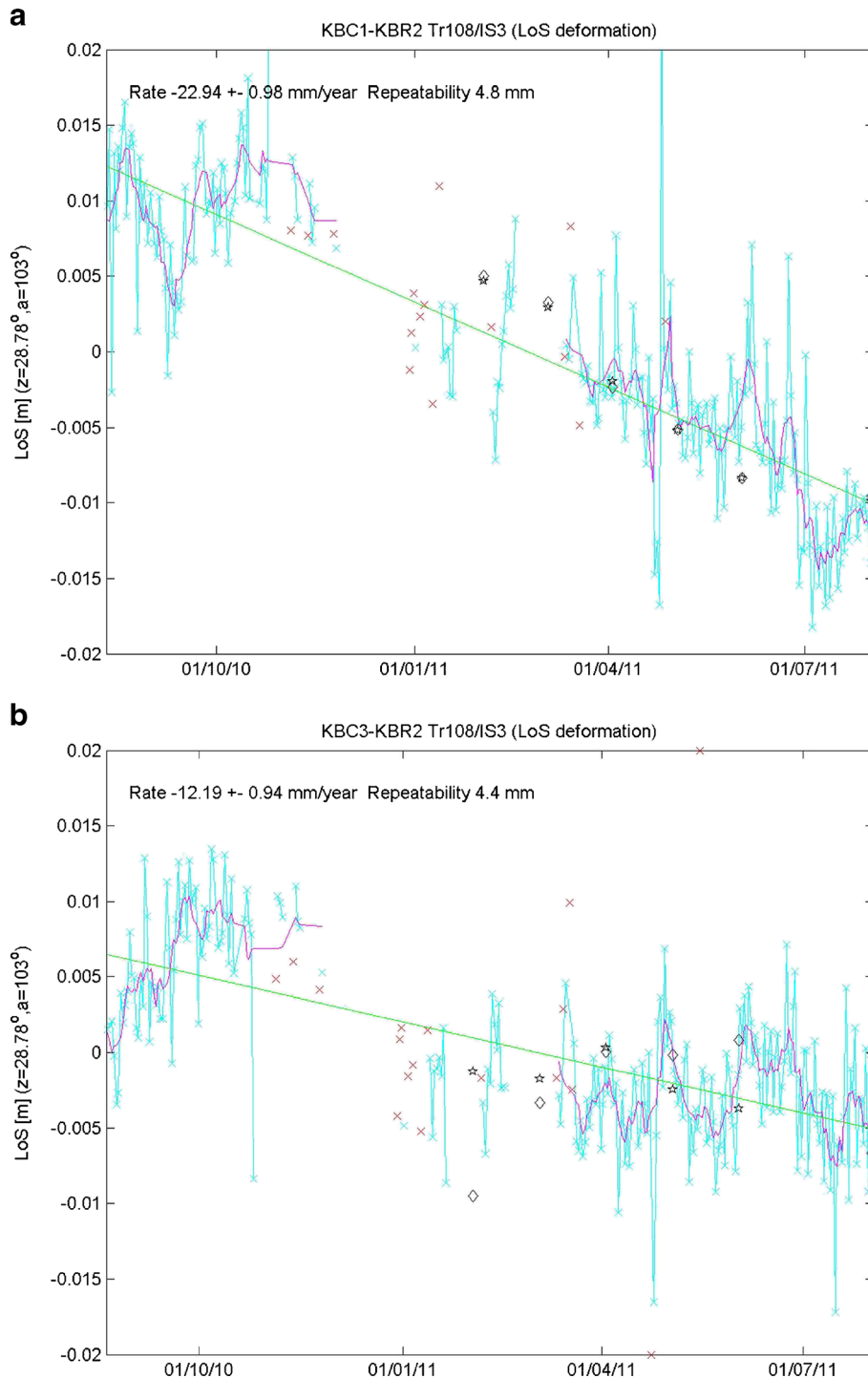|	Vel N	Vel E	Vel Up	Rep N	Rep E	Rep Up
GSR1	3.73	0.88	−1.75	1.1	1.5	3.0
Ref2	−0.06	−0.38	−1.38	1.6	2.1	4.7
CAT1	−22.14	−57.43	0.56	1.8	3.5	6.2
CAT3	−6.01	−13.17	−8.80	2.5	4.4	4.8
Ref2'	0	0	0	0	0	0
CAT1'	−21.99	−57.79	2.04	1.3	1.8	5.7
CAT3'	−6.28	−13.99	−7.19	1.9	2.7	5.0

a

b

Fig. 14 Line of sight deformation for track 108 (IS3) with incidence 28.78°. The *crosses* (*cyan*) are the LOS deformation for GPS; it is the los deformation difference between KBC1 (*top*) and KBC3 (*bottom*) with the reference KBR2. The *magenta curve* is the 7-day running average of the GPS results, and the *green line* is the fitted trend line. The *red crosses* are GPS samples where the receiver did not track the GPS signals for more than 16 h/day. The repeatability is computed after subtracting the yearly velocity. The InSAR deformations are shown as *black diamonds and stars*. The *diamonds* is the deformation computed with respect to the first image, the *stars'* result from the cumulative summing of consecutive pairs of images. The InSAR deformations are aligned to the GPS results through an arbitrary shift computed from the InSAR and GPS difference

InSAR is minimised. This is equivalent to a minimum norm transformation. It should be pointed out that this shift is not 0, on account of the different reference epochs in the GPS and InSAR double differences, and on account that both are measurements.

As reference for the GPS, we took the unsmoothed daily estimates (the cyan curve in the plot). The trend line and 7-day running average have not been included in the comparison. The root mean square (RMS) differences are shown in Table 6.

Table 6 Standard deviation of the difference between GPS/GNSS and PSI displacements

	Single master image	Summing consecutive images
KBC1-KBR2	3.2	3.1
KBC3-KBR2	5.3	5.3

For track 108, the best fitting results are obtained from the InSAR displacements that resulted from the processing with a single master image. The RMS differences are between 2.1 and 3.4 mm. This is compatible with the individual accuracy of the GPS displacements (3 mm) and InSAR displacements (1.3 mm).

When analysing the benefits of linking the integrated GPS/GNSS and InSAR data into the absolute reference system (ITRF2008), two direct benefits could be determined, the first is when GPS/GNSS data is corrected with the InSAR data to enhance the vertical displacements accuracy and the second is when InSAR measurements are added into the GPS/GNSS system to estimate the displacement velocities. Results of the first approach do show significant improvements in vertical displacement measurement accuracy, but these can be only done for the measurements at the time of InSAR data acquisition. The best improvements were achieved with the vertical component of displacements. As GPS/GNSS data are near continuous time series such (sporadic) corrections made with InSAR do not really offer significant improvement of the combined vertical displacements accuracy. We do not recommend the second approach, which only integrates the two measurements at the level of velocity estimates, as adding InSAR to GPS/GNSS had little impact on the horizontal velocities accuracy but also the impact on the vertical velocities accuracy was very small. It is also a highly unreliable approach for non-linear motion that is present at the Potoška planina site (Figs. 12 and 13).

Assessment of the TZD results shows that there were significant effects of the height differences between the stations, and also the effect of the seasons was present. Due to some very inconvenient data gaps at Ref2 in Feb/March 2011, a CAT1 was chosen as a merit for the calculation of the TZD, but as this is performed between points it does not change the results.

The mean and standard deviation of the differences were calculated are summarised in Table 7. In order to get the effect of the troposphere delay in the LOS to the SAR satellites, the differences were multiplied by the same troposphere mapping function as has been used in the GPS/GNSS processing (Niell mapping function; roughly $1/\cos(z)$, where z stands for the incidence angle of SAR signal). The value estimated gradient for track 108 is 1.141.

The standard deviation of the GPS/GNSS atmospheric corrections is estimated at 5–6 mm in the LOS. If these corrections are applied to the InSAR data, the results of the comparison between GPS/GNSS and InSAR do not improve. On the contrary, the RMS differences are worse. This is understandable for the short baseline as the error in the double differenced atmospheric corrections is much larger than the effect itself. But we have not achieved any improvement for the long baselines either. The results are even worse than for the short baselines since the corrections are much larger. In order to find any improvement for the long baselines, we need to also address ambiguity resolution, as it is likely that when atmospheric corrections are applied, this affects the (2.8 cm) ambiguities. The RMS error in the atmospheric corrections was about 5–6 mm in the LOS. If we applied these corrections to the InSAR data, the precision of the InSAR displacements was also reduced to 5–6 mm accuracy, which was worse than the GPS displacements.

It would only be useful to apply atmospheric corrections if the accuracy of the corrections would be around 1–2 mm at most. In order to obtain this quality for the atmospheric corrections and to reduce errors, if possible at all, we would need to do advance atmospheric modelling, smoothing or only consider the systematic contribution. Hence, the conclusion is that the application of instantaneous atmospheric corrections from GPS has not been successful as they are too noisy.

It was also anticipated that co-located GPS/GNSS measurements would be advantageous for resolution of potential wrapping ambiguities in InSAR measurements. The trial results showed that this is indeed possible. However, given the greater temporal sampling and availability of a 3D motion vector, it would appear that there is little added benefit from this at points where high-accuracy continuous GNSS measurements are already available. There could be potential added value to use the GPS/GNSS measurements to resolve ambiguities of nearby non-GNSS artificial reflectors in addition to those at the co-located unit. However, this would depend on the spatial continuity of the motion phenomenon being observed. The close correspondence of InSAR motion measurements for the adjacent CAT1 and CAT4 could indicate that this spatial continuity may be present in some parts of the Potoška planina landslide.

The benefits of integrated processing can be considered in terms of the mutual benefits of each technique to the other.

Given the greater temporal sampling and availability of a 3D motion vector, it would appear that there is little added benefit from the addition of an InSAR capability where high-accuracy continuous GNSS measurements are available. It is often stated that GNSS has insufficient vertical accuracy in comparison to InSAR; however, results from this trial show that high-specification continuous GNSS equipment and expert processing can give vertical accuracies approaching those of InSAR.

Addition of co-located GNSS to InSAR measurements does enhance the capabilities of InSAR with regard to resolution of motion ambiguities. However, this is of little benefit at the co-located point since the GNSS measurements are already providing an accurate 3D motion vector at that location. There could be scope in some situations to use the GNSS measurements to resolve ambiguities of nearby artificial reflectors, although this will depend on the spatial continuity of the motion phenomenon being observed. Field trial results show that GNSS-derived atmospheric corrections are too noisy in order to be useful to correct InSAR data without any additional modelling. Addition of GNSS equipment at numerous locations also involves installation of costly ground infrastructure, negating the low-cost remote wide-area monitoring advantages of the InSAR technique.

Table 7 Mean and standard deviation of the TZD differences with respect to CAT1

	Mean (mm)	STD (mm)
Ref2-CAT1	23.7	4.1
CAT3-CAT1	28.4	4.6

It is felt that the largest possible benefit of integrating InSAR and GNSS is the provision of an absolute reference point to tie relative InSAR results into conventional geodetic reference systems. This would leverage the wide-area remote monitoring capabilities of conventional InSAR techniques, while limiting the GNSS equipment cost to a small number of units. Deployment of a number of co-located GNSS and artificial reflector units could also have potential for mitigating orbital trends in InSAR results.

A requirement for the integrated processing discussed above is that there is a fixed relation between the phase centres of the GNSS antenna and the artificial reflector, and that this relationship does not change in time. The advantage of the I2GPS unit and associated mounting structure used in this work is that it provides a mechanism to ensure such a relationship should be repeatable even after unit removal and replacement. It also defines a standard such that this relationship could be kept identical across multiple I2GPS units and sites.

Conclusions

As the approach presented in this paper was the first known attempt to combine continuous GPS/GNSS and InSAR active transponders in a co-registered system (the same baseplate), there were number of challenges to be overcome during the work. At the same time, such an attempt was unique to our knowledge in the field of landslide monitoring. Despite obstacles listed in the paper, it can be concluded that there are two immediate benefits of integrating InSAR with GPS/GNSS, and these are (1) displacements in an absolute reference frame for all CATs and I2GPS units, as long as there is one I2GPS unit in the network, and (2) improved 3D displacement vectors for all I2GPS units in the network.

References

Borgeaud M, Wegmüller U (1997) On the use of ERS SAR interferometry for the retrieval of geo- and bio-physical information. In: Guyenne TD, Danesy D (eds) Proceedings of the 'Fringe 96' workshop on ERS SAR interferometry. ESA, Zürich, Switzerland, pp 83–94

Bossler JD, Goad CC, Bender PL (1980) Using the global positioning system (GPS) for geodetic surveying. Bull Géod 54:553–563

Bovenga F, Nutricato R, Refice A, Wasowski J (2006) Application of multi-temporal differential interferometry to slope instability detection in urban/peri-urban areas. Eng Geol 88:218–239

Bruyninx C (2004) The EUREF permanent network: a multi-disciplinary network serving surveyors as well as scientists. GeoInformatics 7:32–35

Carnec C, Delacourt C (2000) Three years of mining subsidence monitored by SAR interferometry, near Gradane. J Appl Geophysics 43:43–54

Crosetto M, Gili JA, Monserrat O, Cuevas-Gonzalez M, Corominas J, Serra D (2013) Interferometric SAR monitoring of the Vallcebre landslide (Spain) using corner reflectors. Nat Hazards Earth Syst Sci 13:923–933

Dach R, Hugentobler U, Fridex P, Meindl M (2007) Bernese GPS software 5.0. Astronomical Institute, University of Berne

Declerq PY, Devleeschouwer X, Pouriel F (2005) Subsidence revealed by PSInSAR technique in the Ottignies-Wavre area (Belgium) related to water pumping in urban area. In: Lacoste H, Ouwehand L (eds) Proceedings of Fringe 2005 Workshop, 28 November–2 December 2005, Frascati, Italy (ESA SP-610, February 2006). European Space Agency, Noordwijk, Netherlands, pp 66.1–66.6

Dow JM, Neilan RE, Rizos C (2009) The International GNSS Service in a changing landscape of Global Navigation Satellite Systems. J Geod 83:191–198

ESA SP-1322/1 (2012) Sentinel-1: ESA's radar observatory mission for GMES Operational Services. Ed. K. Fletcher, ISBN 978-92-9221-418-0. http://esamultimedia.esa.int/multimedia/publications/SP-1322_1/.

Farina P, Colombo D, Fumagalli A, Marks F, Moretti S (2006) Permanent scatterers for landslide investigations: outcomes from the ESA-SLAM project. Eng Geol 88:200–217

Ferretti A, Prati C, Rocca F (2000) Nonlinear subsidence rate estimation using permanent scatterers in differential SAR interferometry. IEEE T Geosci Remote Sens 38:2202–2212

Ghiglia DC, Pritt MD (1998) Two-dimensional phase unwrapping: theory, algorithms, and software. Wiley, New York. ISBN ISBN-13: 978-0471249351

Ketelaar G, Marinkovic P, Hanssen R (2004) Validation of point scatterer phase statistics in multi-pass InSAR. In Proc. CEOS SAR Workshop, pp. 27–28.

Hilley GE, Bürgmann R, Ferretti A, Novali F, Rocca F (2004) Dynamic of slow-moving landslides from permanent scatterer analysis. Science 304:1952–1955

Hole J, Holley R, Giunta G, De Lorenzo G, Thomas A (2011) InSAR assessment of pipeline stability using compact active transponders. In: Proceedings of FRINGE2011, 8th International Workshop on "Advances in the Science and Applications of SAR Interferometry". European Space Agency, Frascati, Italy, p 201, 19–23 September 2011

Hooper A, Zebker H, Segall P, Kampes B (2004) A new method for measuring deformation on volcanoes and other natural terrains using InSAR persistent scatterers. Geophys Res Lett 31:L23611, doi:10.1029/2004GL021737

Ježak J, Mikoš M, Trajanova M, Kumelj Š, Bavec M (2008) Vršaj Koroška Bela–Rezultat katastrofičnih pobočnih dogodkov = Koroška Bela alluvial fan - the result of the catastrophic slope events (Karavanke Mountains, NW Slovenia). Geologija 51(2):219–227

Komac M, Bavec M (2007) Application of PS InSAR for observing the vertical component of the recent surface displacement in Julian Alps. Geologija 50(1):97–110

Ludwig R, Schenider P (2006) Validation of digital elevation models from SRTM X-SAR for applications in hydrologic modeling. ISPRS J Photogramm 60:339–358

MacDonald, Dettwiler and Associates Ltd. (2004) RADARSAT-1 data products specifications RSI-GS-026, Revision 3/0. http://gs.mdacorporation.com/includes/documents/R1_PROD_SPEC.pdf.

MacDonald, Dettwiler and Associates Ltd. (2011) RADARSAT-2 Product Description RN-SP-52-1238 Issue 1/9. http://gs.mdacorporation.com/includes/documents/RN-SP-52-1238_RS2_Product_Description_Iss1-9.pdf.

Mahapatra P, Hanssen R, Van der Marel H, Chang L, Dheenathayalan P, Delgado Blasco J-M, Esteves Martins J, Holley R, Komac M, Prior C, Fromberg A (2011) A comparative study of corner reflectors, compact active transponders and I2GPS for monitoring deformation in areas with low spatial density of persistent scatterers: the Delft field experiment. In: Proceedings of FRINGE2011, 8th International Workshop on "Advances in the Science and Applications of SAR Interferometry". European Space Agency, Frascati, Italy, pp 106–107, 19 – 23 September 2011

Mikoš M, Sodnik J, Podobnikar T, Fidej G, Bavec M, Celarc B, Jež J, Rak G, Papež J (2012) PARAmount—European research project on transport infrastructure safety in the Alps. In: Sassa K, Takara K, He B (eds) Proceedings IPL Symposium Kyoto, 2012: 20 January 2012, Venue: Disaster Prevention Research Institute, Kyoto University Uji, Kyoto, Japan. International Consortium on Landslides, Tokyo, pp 111–118

Miranda N, Meadows PJ, D'Aria D, Giudici D (2009) Status of ERS-2 SAR & Envisat ASAR instruments and products. Presentation at ESA Fringe conference 2009. http://earth.eo.esa.int/workshops/fringe09/participants/781/pres_781_NMiranda.pdf.

Mohr JJ, Madsen SN (1999) Automatic generation of large scale ERS DEMs and displacement maps. Available on CD-ROM: advancing ERS SAR Interferometry from Applications towards Operations. ESA, Noordwijk, The Netherlands

Mueller II, Beutler G (1992) The International GPS Service for Geodynamics—development and current structure. Proceedings of the 6th Symposium on Satellite Positioning. Ohio State University, Columbus, OH, pp 823–835

Remondi BW (1985) Global positioning system carrier phase: description and use. Bull Géod 59(4):361–377

Salvi S, Atzori S, Tolomei C, Allievi J, Ferretti A, Rocca F, Prati C, Stramondo S, Feuillet N (2004) Inflation rate of the Colli Albani volcanic complex retrieved by the permanent scatterers SAR interferometry technique. Geophys Res Lett 31:12606–12610

Squarzoni C, Delacourt C, Allemand P (2003) Nine years of spatial and temporal evolution of the La Vallette landslide observed by SAR interferometry. Eng Geol 68:53–66

Teunissen PJG, Kleusberg A (1998) GPS for geodesy. Springer, Berlin

Werner C; Wegmuller U; Strozzi T; Wiesmann A(2003) Interferometric point target analysis for deformation mapping. Geoscience and Remote Sensing Symposium, 2003. IGARSS '03. Proceedings. 2003 IEEE Int 7:4362, 4364. 21–25 July 2003. doi: 10.1109/IGARSS.2003.1295516.

Žibret G, Komac M, Jemec M (2012) Assessing the relation between PSInSAR displacements (related to soil creep) on unstable slopes and rainfall intensities in western Slovenia. Geomorphology 175–176:107–114. doi:10.1016/j.geomorph.2012.07.002

M. Komac (✉) · M. Bavec
Geological Survey of Slovenia,
Ljubljana, Slovenia
e-mail: marko.komac@geo-zs.si

R. Holley
CGG NPA Satellite Mapping Limited,
Edenbridge, UK

P. Mahapatra · H. Marel
Delft University of Technology,
Delft, The Netherlands